Evaluation of Fractal Dimension effectiveness for damage detection in retinal background

Adrián Colomer[a,b,*], Valery Naranjo[a,b], Thomas Janvier[c], Jose M. Mossi[d]

[a] *Instituto de Investigación e Innovación en Bioingeniería (I3B), Universitat Politècnica de València, Camino de Vera s/n, 46022, Valencia, Spain.*
[b] *Grupo Tecnologías de Informática Aplicadas a la Oftalmología, Unidad Conjunta UPV-FISABIO, Spain.*
[c] *University of Orléans, I3MTO Laboratory, Rue de Chartres, BP 6759, 45067 Orléans Cedex 2, France.*
[d] *ITEAM Research Institute, Universitat Politècnica de València, Camino de Vera s/n, 46022, Valencia, Spain.*

Abstract

This work investigates the characterization of bright lesions in retinal fundus images using texture analysis techniques. Exudates and drusen are evidences of retinal damage in diabetic retinopathy (DR) and age-related macular degeneration (AMD) respectively. An automatic detection of pathological tissues could make possible an early detection of these diseases. In this work, fractal analysis is explored in order to discriminate between pathological and healthy retinal texture. After a deep preprocessing step, in which a spatial and colour normalization are performed, the fractal dimension is extracted locally by computing the Hurst exponent (H) along different directions. The grayscale image is described by the increments of the fractional Brownian motion model and the H parameter is computed by linear regression in the frequency domain. The ability of fractal dimension to detect pathological tissues is demonstrated using a home-made system, based on fractal analysis and Support Vector Machine, able to achieve around a 70% and 83% of accuracy in E-OPHTHA and DIARETDB1 public databases respectively. In a second experiment, the fractal descriptor is

*Corresponding author at Universitat Politècnica de València, I3B, Spain
Email addresses: adcogra@i3b.upv.es (Adrián Colomer), vnaranjo@i3b.upv.es (Valery Naranjo), thomas.janvier@univ-orleans.fr (Thomas Janvier), jmmossi@dcom.upv.es (Jose M. Mossi)

combined with texture information, extracted by the Local Binary Patterns, improving the bright lesion detection. Accuracy, sensitivity and specificity values higher than 89%, 80% and 90% respectively suggest that the method presented in this paper is a robust algorithm for describing retina texture and can be useful in the automatic detection of DR and AMD.
Keywords: Retinal fundus image, Fractal analysis, Diabetic retinopathy, Age-related macular degeneration, Local Binary Patterns.

1. Introduction

Diabetic retinopathy (DR) and age-related macular degeneration (AMD) are two of the most common pathologies in the current society that provoke retinal damage and can be directly related to blindness and vision impairment. Although in recent years the number of cases has been significantly reduced, it is estimated that the 80% of cases of visual impairment is preventable or treatable. The early diagnosis of these pathologies allows to reduce costs generated when they are in advanced states and may become into chronic. Due to the large of population at risk, a potential automatic screening would highly benefit to clinicians reducing the workload of trained experts in the analysis of anomalous patterns of each disease.

Retinal fundus images are the most non-invasive acquisition modality in which different lesions are manifested; these lesions are the basis to identify the pathologies and their stage of proliferation. Figure 1 shows the distinctive lesions evidenced in pathological fundus images. This work is focused on the automatic detection of the bright lesions that characterize DR and AMD, exudates and drusen respectively.

In the literature, the most common procedure is to segment these lesions using different methods [1–3] but in this work the characterization of the healthy and the pathological retina is studied applying texture analysis techniques, in particular, fractal descriptors, avoiding the segmentation step.

Fractal objects are characterized by a high degree of complexity but also by

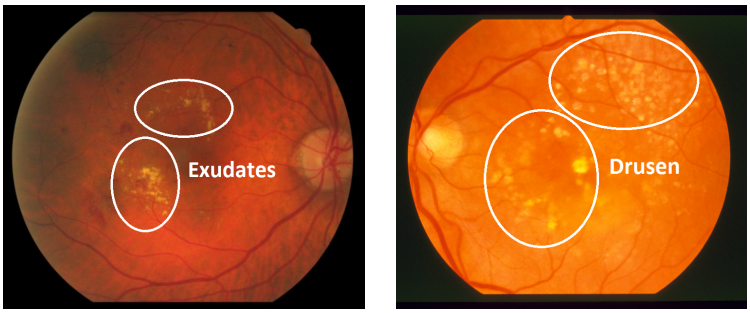

(a) (b)

Figure 1: (a) Lesions of Diabetic Retinopathy and (b) signs of age-related macular degeneration.

self-similarity represented by a repetition of patterns or statistical properties over different scales. Based on this property of self-similarity it is possible to describe an image by means of a fractal dimension (FD) parameter. The characterization of gray level images is described using the potential usefulness of the fractional Brownian motion (fBm) model [4].

Fractals have been recognized as an effective descriptor of complex structures in biology and medicine [5]. In the literature, fractal analysis have been proposed for characterizing biomedical signals and images [6–10]. Regarding to retinal fundus images, fractals have only been applied to the retinal blood vessels characterization. In [11], a fractal analysis approach based on the box-counting method was used to quantify vascular patterns in normal and abnormal cases showing neovascularization (caused by proliferative diabetic retinopathy in advanced stages of the disease). The algorithm was validated in ten images. In [12], a blood vessel segmentation method based on fractal analysis was proposed and a comparison of the fractal dimension (extracted from the blood vessels) between hypertension and non-hypertension groups was carried out without significant evidences of discrimination ability. The authors of [13] proposed a semi-automatic method to compute the fractal dimension of fundus images. They established a comparison between their method and the box-counting method. Finally, the authors applied the proposed algorithm with the

aim of testing the impact in the variation of blood vessels due to the angle between the acquisition camera and the optical axis. To the best of the authors' knowledge, fractal analysis has not been used previously in the characterization of retinal lesions and it could be a key factor because exudates and drusen are the first recognizable signs of the diseases under study.

The main objective of this work is to demonstrate that the fBm model suits well for the characterization of pathological texture in retinal images and as novelty we demonstrate how it is possible to detect bright lesions by means of the fractal dimension. In addition, fractal dimension will be combined with another texture descriptor in order to enhance the yield of a computer-aided diagnosis system developed by the authors.

The rest of the paper is organized as follows: in Section 2, the fractional Brownian motion model able to describe the fractal dimension in grayscale images is explained. In addition, an explanation about how the fractal descriptor is extracted from the retinal texture is detailed. Section 3 shows, on the one hand, a statistical analysis of the fractal dimension according to the healthy and pathological retinal texture. On the other hand, the results of the automatic detection of bright lesions on two public fundus databases, using the home-made system, are presented. Finally, section 4 provides conclusions and some areas for future work.

2. Material and methods

2.1. Material

The validation of the proposed method was carried out on two public public databases. E-OPHTHA database [14] is divided in two subsets depending on the lesion type: exudates and microaneurysms. These lesions are manually annotated by experts and the ground-truth is provided. The exudates subset (E-OPHTHA_EX) used in this work is composed by forty seven retinal images of different spatial resolutions (see Table 1) acquired with the same field of view

angle, i.e. 40. Due to this resolution variety, a stage of spatial normalization is essential.

Image resolution (pix.)	1440×960	1504×1000	2048×1360	2544×1696
Number of images	13	2	9	23

Table 1: Distribution of the E-OPHTHA_EX images with exudates according to their resolution.

DIARETDB1 public database [15] consists of 89 colour fundus images, of which 47 contain exudates. Images were captured using the same 50 degree field-of-view digital fundus camera and all images present a resolution of 1500×1152 pixels. The 89 images of this database were marked by four experts. These annotations are provided as a probability map. The procedure proposed by the authors of DIARETDB1 to generate the ground truth images from the probability map, is follow in this work. Each pixel marked as exudate by 3 of the 4 experts is considered as exudate pixel in the binary mask.

Note that a list with the original images used as well as the resulting source code implemented of this work is publicly available in `https://github.com/adcogra/Fractal_Analysis_JCAM` to reproduce and verify the obtained results facilitating future fair comparisons.

2.2. Fractals

The minimum number of independent variables to describe an object is defined by the Euclidean dimension (E). A point is a 0-dimensional object; a line is 1-dimensional while a plane is 2-dimensional. However, this approach does not extract information about the "roughness" of the object, in other words, Euclidean dimension of a line will always remain constant (E=1) whatever it is straight or crooked.

Two centuries ago different mathematicians such as Koch, Sierpinski and Hausdorff established a geometric definition of fractals demonstrating that shapes and objects have fractional dimension. Fractals objects are built based on a

pattern repeated at different scales and can therefore be described as a part of themselves. This property illustrated in Figure 2 is known as "self-similarity".

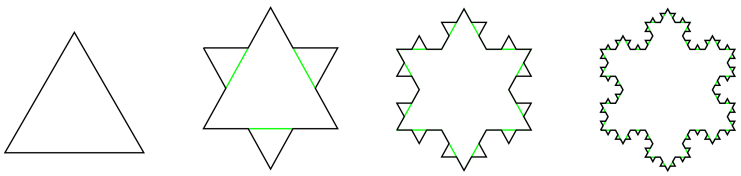

Figure 2: The first four iterations of the Koch snowflake.

To characterize such objects, a non-integer dimension is used: the fractal dimension (FD). However, this term does not reflect a single descriptor, as several definitions coexist. The simplest way to apprehend the FD is using the homothety a.k.a. similarity dimension (D_H):

$$D_H = \frac{\ln(N)}{\ln(r^{-1})} \tag{1}$$

where N is the number of elementary patterns included in the object and r is their reduction factor. This computation is valid only for a geometrical set with internal homotheties, and can be extended to any set using the box-counting a.k.a. Minkowski-Bouligand dimension (D_B):

$$D_B = \lim_{\epsilon \to 0} \frac{\log(N_\epsilon)}{\log(\epsilon^{-1})} \tag{2}$$

where N_ϵ is the minimal number of subsets with a size ϵ required to cover the object. This FD reflects the complexity of the object and its construction. In particular, a signal with higher FD is more complex or rough than a signal with lower FD.

Another popular way to define the fractal dimension concept is the so-called *capacity*(D_C). This definition makes reference to the characterization of fractal patterns or sets by quantifying their complexity as a ratio of the change in detail to the change in scale [16]. The relation between the length of an object and its

roughness is given by:

$$L_\delta = K \cdot \delta^{(1-D_C)} \tag{3}$$

where L_δ is the length of the object, δ the measuring scale, K a constant and D_C the object fractal dimension (FD).

2.3. Fractional Brownian motion model

In the work presented by Mandelbrot and Van Ness [17], fractional Brownian motion is defined by its stochastic representation based on the long-range dependence and self-similar behaviours. This representation is governed by a single parameter called the Hurst exponent (H) [18] which is linked to the fractal dimension by $H = E + 1 - FD$, where E is the Euclidean dimension. Due to the random nature of fundus lesions in terms of location, shape and size (see Section 1), the fractal model based on fBm is used to describe these random phenomena [19]. In the following lines, the fractional Brownian motion model is formulated to be applied in grayscale images.

The spectral representation of fBm, $B_H(t)$, is given by [20]:

$$B_H(t) = \frac{1}{2\pi} \int_{-\infty}^{+\infty} \frac{1}{(\mathrm{i}\omega)^{H+1/2}} (e^{\mathrm{i}t\omega} - 1) dB(\omega) \tag{4}$$

where $B_H(t)$ is a Gaussian, continuous, centered and non-stationary second-order process, ω designates the set of all values of a random function (where ω belongs to a sample space Ω), $dB(\omega)$ is the white noise integration corresponding to the Gaussian process and t refers time and it ranges in the interval $(-\infty, +\infty)$.

Applying the initial condition $B_H(0) = 0$, its covariance function (ρ) is given by:

$$\rho(s,t) = E[B_H(s)B_H(t)] = \frac{a^2 V_H}{2}(|t|^{2H} + |s|^{2H} - (t-s)^{2H}) \tag{5}$$

for $0 < s <= t$ where $E[\cdot]$ is the mathematical expectation, a is a constant and

V_H a function of H defined as [21]:

$$V_H = \Gamma(1-2H)\frac{cos(\pi H)}{\pi H} \tag{6}$$

where Γ is the gamma function.

The self-similarity property of the fBm can be expressed as:

$$B_H(km) \equiv k^H B_H(m); \qquad \forall k \quad and \quad m > 0 \tag{7}$$

As fBm is a non-stationary process, it is more convenient to study its incremental process called fractional Gaussian noise (fGn), defined as the derivative of fBm at a resolution m:

$$G_m(k) = B_H(k) - B_H(k-m) \tag{8}$$

The corresponding autocovariance function $\gamma(\cdot)$ is given by:

$$\gamma(\tau) = E[G_m(k)G_m(k+\tau)] = \frac{\sigma_m^2}{2|m|^{2H}}(|\tau+m|^{2H} + 2|\tau|^{2H} + |\tau-m|^{2H}) \tag{9}$$

where $\sigma_m^2 = a^2 V_H |m|^{2H}$ is the variance of G_m.

For fGn class signals, the probability distribution of a segment of the signal is independent of the segment size and its temporal position in the signal [22]. This property plays an important role in this work due to a local computation of the fractal dimension is performed as detailed in the following subsection.

The Power Spectra Density (PSD) of the fGn can be calculated from (9), and when m tends to infinity, a normalized spectrum of the fBm increments can be defined as [23]:

$$PSD_{G_m}(f) \propto |f|^{1-2H} \tag{10}$$

In this work, the fGn-based Spectral Estimator (GSE) is used in order to compute the parameter H from the PSD of the fBm increments. Equation (10) shows that the PSD follows a law in $|f|^{1-2H}$. In a log-log scale, the PSD

function of the fBm increments is a line of slope $1 - 2H$. The H parameter can be estimated by linear regression. Regarding to the GSE implementation, the average spectrum of the fGn is estimated for each patch by the square of the modulus of the Fourier transform computed by the Fast Fourier Transform (FFT) algorithm.

2.4. Application to retinal images

As we introduced in section 1, the main novelty of this work is to apply fractal analysis in order to model the healthy retinal texture and the bright retinal lesions produced by DR and AMD. With the aim of reliably obtaining the fractal description of both tissues reliably, an image preprocessing step is essential before the local fBm computation and the Hurst exponent estimation.

2.4.1. Retinal fundus image preprocessing

Public fundus images belonging to a specific database can present different resolutions due to the configuration of the retinal camera. This fact can hinder the comparison of the lesions and anatomical structures. E-OPHTHA_EX database is composed by images with four different resolutions as we mentioned in section 2.1. For this reason, the first preprocessing step is a spatial normalization. The images are resized to the dimensions of the smallest image (1440×960) after a local maximum filter applied in order to preserve the small bright lesions.

Another uncalibrated factor in fundus images is the background colour due to the retina variability. Retinal fundus colour depends on age, ethnicity, differences in retina pigmentation and other anatomical human factors. In order to avoid problems in the fractal description due to these factors, a colour normalization of the images is performed (Figure 3(b)). In particular, a colour normalization based on geometric tranformations applied to the chromatic histogram of the image [24] is performed.

Blood vessels cover a high percentage of the fundus image and are considered as noise or artefacts that hamper the classification of pathologies based on

background textures. For this reason it is necessary to remove the contribution of this structure to the fractal analysis. Retinal vessels are detected using the algorithm proposed by Morales et al. [25]. This method is based on mathematical morphology and curvature evaluation for the detection of retinal vascular tree (Figure 3(d)). A possible procedure to avoid blood vessels is to consider these structures as missing pixels and trying to restore them using the background. This technique is known as image inpainting and different kind of methods exist in the literature. In this paper, the diffusion-based inpainting method by means of the simplest isotropic diffusion model is used with the implementation proposed in [26]. Figure 3(e) shows a retinal inpainted image, the input to the fractal analysis stage.

In fundus images, the green component of the RGB-representation shows the maximum contrast between lesions and background, the red channel is often saturated and has low contrast, and the blue channel is very noisy and suffers poor dynamic range. For these reasons, the green component is commonly used to segment the lesions [1, 27, 28] and it is used in this work (Figure 3(f)).

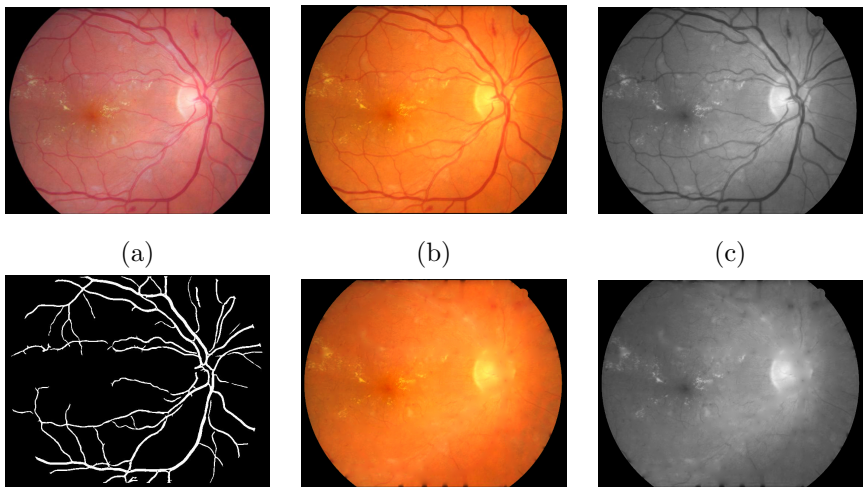

Figure 3: Retinal fundus image preprocessing. (a) Original image, (b) colour-normalized image, (c) green component of the normalized image, (d) vessel mask extracted using [25], (e) inpainted image without blood vessels and (f) input image to the fractal analysis stage.

2.4.2. Local computation of the fractal dimension

The lesions induced by macular degeneration or diabetic retinopathy present different sizes according to the stage of the disease. In most cases, lesions represent less than one percent of the total number of pixels that compose the retinal image. For this reason, in the feature extraction stage, fractal dimension is performed locally, in other words, the image is divided in patches using a sliding window (Figure 4(a)) and the texture descriptor is computed for each patch. The window used is a square of canonical size (N_w) with overlap of (Δx,Δy). Note that patches containing optic disk pixels [29] are not considered in the process. Patches should also be completely contained within the field of view of the retinal image (Figure 4(b)).

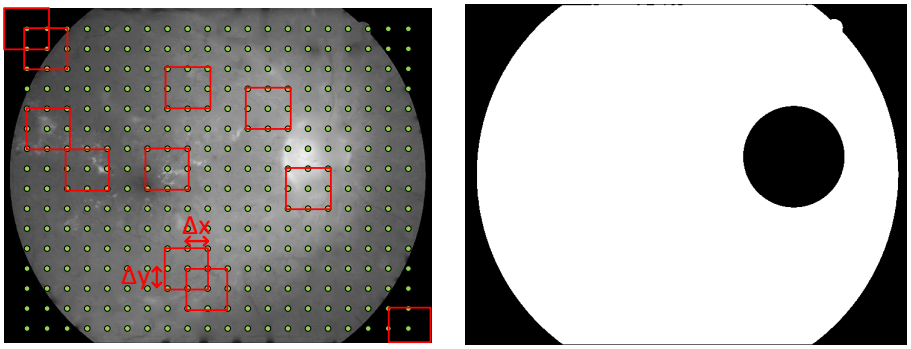

(a) (b)

Figure 4: (a) Image grid indicating the positions of the sliding windows ($N_w = 64$) using (Δx,Δy) = (32,32) and (b) binary mask used in order to exclude the patches containing optic disk pixels or the patches located out of the field of view.

In this work fractal dimension of 2D image patches is extracted. With the aim of reducing the loss of information, a multi-dimensional extension of the fBm is used by means of the multiparameter Wiener process, or Brownian sheet presented in [30]. An anisotropic extension of the fGn allows the extraction of different Hurst exponents, one parameter in each of the L directions, gathered in the vector parameter $H = (H_1, H_2, ..., H_L)$. In particular, the Hurst parameter in L = 2 directions (0 and 90 degrees) is computed from the average PSD (in

each direction) and stacked as a vector $H = [H^{0^\circ}, H^{90^\circ}]$.

Let X be an image patch of dimensions $M \times N$, for each row m we obtain the 1D signal $d[n] = X[m, n+1] - X[m, n]$ and compute the discrete Fourier transform given by:

$$D[k] = \sum_{n=0}^{N-1} d[n] e^{\frac{-j2\pi kn}{N}} \tag{11}$$

These 1D spectra compound the M rows of a 2D matrix $D'[k, l]$. Finally, the PSD is computed by a pointwise averaging in each column as:

$$PSD[k] = \frac{1}{M} \sum_{l=0}^{M-1} D'[k, l] \tag{12}$$

Figure 5(a) shows a patch extracted from the retina background of the image displayed in Figure 4; the white arrow defines a specific patch row in which the intensity is studied. We can notice the non-stationarity of this intensity signal (Figure 5(b)) along the patch width. As recalled above, the increments of the intensity are easier to study due to their stationarity (Figure 5(c)). In Figure 5d it is possible to observe the $\overline{PSD}^{0^\circ}$ extracted from the patch under study by means of equation (12).

Finally, in order to extract the H parameter of the patch, a linear regression in log-log scale for the PSD curve (Figure 5(d)) is performed and the Hurst exponent is estimated using equation (10). Linear regression is performed in the frequency interval $f \in [f_{ini}, f_{end}]$ in which the PSD curve, plotted in a log-log scale, is linear. This linear behaviour shows the fractal nature of the tissue under study. The intergroup roughness of image patches is quite different, in other words, the linear segment in the log-PSD curve for patches labelled as healthy and pathological is located in a different frequency interval. However, this range of frequencies is quite similar between patch images of the same class (i.e. low intragroup deviation). These facts allow the automatic computation of the optimal frequency range for each category. Two representative subsets of image patches containing N_h healthy patches and N_p pathological patches respectively are extracted from the training set. For each patch of both subsets,

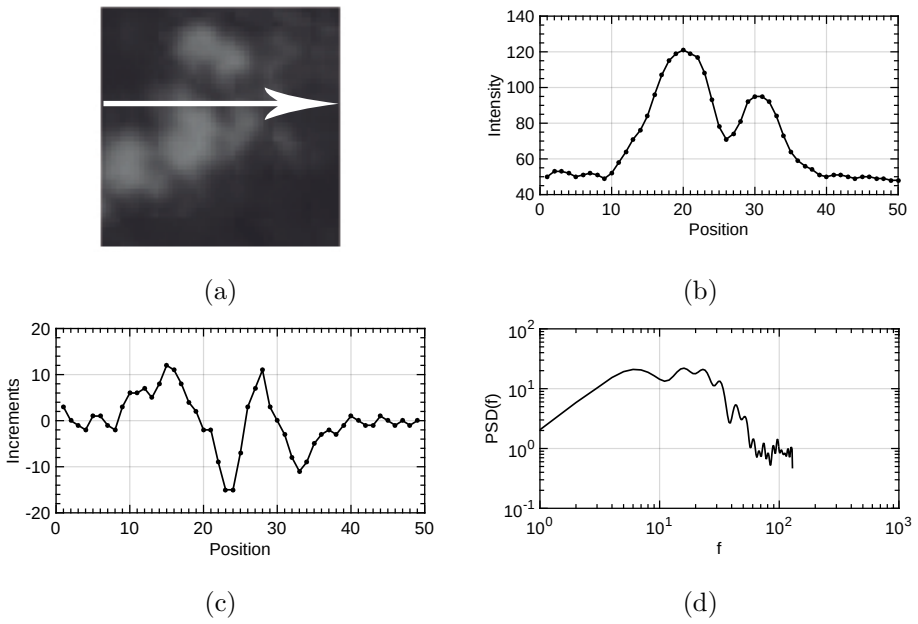

Figure 5: (a) A pathological ROI extracted from a retinal image, (b) the intensity of each pixel extracted from the ROI according to the arrow, (c) the increments of the line presented and (d) the periodogram of the increments of all lines of the ROI.

the optimal frequency range is manually selected $f_i = [f_{ini_i}, f_{end_i}]$ where i ranges between 1 and N_p or N_h depending on the subset. Thanks to the low intragroup deviation, two frequency ranges of reference $f'_h = [f_{h_{ini}}, f_{h_{end}}]$ and $f'_p = [f_{p_{ini}}, f_{p_{end}}]$ can be computed from each subset of the selected frequencies $\Omega_h = \{f_1, f_2, ..., f_{N_h}\}$ and $\Omega_p = \{f_1, f_2, ..., f_{N_p}\}$ as the minimum f_{ini_i} and maximum f_{end_i} respectively. These frequency ranges of reference are used in the automatic computation of the fractal dimension. For each image patch, the curvature inside both frequency ranges is calculated. The frequency range in which the log-PSD curvature is minimum is the frequency range selected to carry out the linear regression.

Algorithm 1 describes the complete process to locally estimate the fractal dimension in $L = 2$ directions from grayscale fundus images.

Algorithm 1: Local fractal analysis computation

Data: RGB fundus image $\mathbf{f} = (f_r, f_g, f_b)$ is the pre-processed retinal image as it was detailed in Section 2.4.1, optic disc mask $\mathbf{M_{od}}$, external mask $\mathbf{M_{ext}}$, size of the sliding window $\mathbf{N_w}$, vectors $\mathbf{r}$ and $\mathbf{c}$ containing the y and x coordinates of the centres of the patches in which the local analysis is performed.

Result: Hurst exponent matrix $\mathbf{H}$ containing the fractal dimension in two directions per patch.

Inicialization:

$ind \leftarrow 1$;

Green channel selection:

$f_{in} \leftarrow f_g$;

Mask computing:

$M \leftarrow and(M_{od}, M_{ext})$

Local fractal analysis:

for $i \leftarrow 1$ **to** $length(\mathbf{r})$ **do**

  for $j \leftarrow 1$ **to** $length(\mathbf{c})$ **do**

    $M^{\diamond} \leftarrow M^{N_w}(r_i, c_j)$;

    $f_{in}^{\diamond} \leftarrow f_{in}^{N_w}(r_i, c_j)$;

    if $\sum_x \sum_y M^{\diamond} > 0$ **then**

      $PSD^{0^\circ} \leftarrow PSD(f_{in}^{\diamond})$;

      $PSD^{90^\circ} \leftarrow PSD(rotate(f_{in}^{\diamond}, 90))$;

      $\overline{PSD}^{0^\circ} \leftarrow mean(PSD^{0^\circ})$;

      $\overline{PSD}^{90^\circ} \leftarrow mean(PSD^{90^\circ})$;

      $\widehat{\overline{PSD}}^{0^\circ} \leftarrow polyfit(\log_{10}(\overline{PSD}^{0^\circ}))$;

      $\widehat{\overline{PSD}}^{90^\circ} \leftarrow polyfit(\log_{10}(\overline{PSD}^{90^\circ}))$;

      $H^{0^\circ} \leftarrow [-0.5(slope(\widehat{\overline{PSD}}^{0^\circ}) - 1)]$;

      $H^{90^\circ} \leftarrow [-0.5(slope(\widehat{\overline{PSD}}^{90^\circ}) - 1)]$;

      $H_{ind} \leftarrow [H^{0^\circ}, H^{90^\circ}]$;

      $ind \leftarrow ind + 1$;

  end

end

2.4.3. Classification process

After the feature extraction stage, the Support Vector Machine (SVM) classifier [31] using the Bootstrap Aggregating (Bagging) technique [32] is used to

classify each patch, extracted from an image, in healthy or pathological according to its fractal dimension. SVM maximises the distance between the hyperplanes defined by specific samples, called support vectors, with the aim of finding the optimal separation between classes. It is important to note that SVM algorithm is applied using the kernel trick technique [33]. In this technique, a specific non-linear function (Φ) is used for mapping non-linear separable data points ($\Omega = \{x_1, x_2, ..., x_n\}$; points $x_i \in \Re^d$) in the original space Σ, into a higher dimensional space in which the data is linearly separable. When this hyperplane of separation is projected back to the input space (Σ), it has the form of a non-linear curve. The new feature space can be of unlimited dimension and thus the hyperplane separating the data can be very complex. The function $K(x, x_i) = \Sigma(x)^T \Sigma(x_i)$ is known as kernel function and in this work, each SVM model is trained using a gaussian kernel (i.e. a Radial Basis Function kernel) defined by the following expression:

$$K(x, x') = \left(\frac{\|x - x'\|^2}{2\sigma^2} \right) \tag{13}$$

where $\sigma \in \Re$ is a kernel parameter and $\|x - x'\|$ is the dissimilarity measure.

Combining the SVM method with the Bagging technique it is possible to improve the stability and accuracy of the machine learning algorithm, reducing the variance and avoiding the overfitting. In this work, the Bagging technique is also used to solve the problem of the unbalanced classes caused by the different number of healthy and pathological patches extracted from a retinal fundus image. Given T pathological patches and K healthy patches where $K >> T$, the bagging technique can be applied in order to balance the classes. In first place, a random permutation of the healthy patches is carried out. After that, M different SVM models can be trained using groups of L healthy patches and the L pathological patches. The final number of classifiers can be calculated as $M = round\,(K/L)$.

An overview of the proposed method is presented in Figure 6. The flow chart shows the different steps of the pre-processing and feature extraction stages.

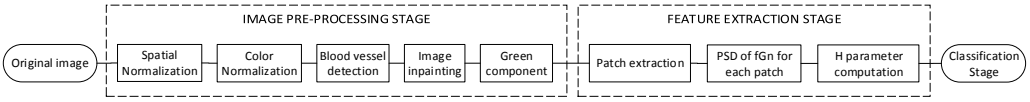

Figure 6: Flow chart of the pre-processing and fractal analysis stages.

3. Results

3.1. Statistical significance analysis of the fractal dimension

The main purpose of this work is to analyse the ability of fractals to discriminate between pathological and healthy retina. For this reason, in the first experiment a statistical analysis of the fractal dimension, described by the Hurst exponent variable, is carried out.

From the 47 color fundus images with exudates of the E-OPHTHA_EX database, 10991 healthy and 2151 patches with lesion are extracted. Figure 7(a) shows the average PSD of the fGn computed from each labelled patch. As it can be observed, the lines that describes these curves (red and green) will be characterized by different slopes and these slopes will define the H parameter or fractal dimension.

The statistical significance of the fractal dimension variable according to the two populations under study is analysed by means of the students t-test [34]. A random selection of 2151 healthy patches is carried out in order to balance the groups. Figure 7(b) shows the box comparison of H parameter. The p-value obtained from the t-test $p < 0.001$ is statistically highly significant, so this fact is promising in order to use the fractal analysis to detect automatically the bright lesions typical in DR and AMD retina background.

3.2. Automatic exudate detection using fractal analysis

An automatic system combining the different stages detailed in Figure 6 was developed by the authors. This computer-aided diagnosis system is used with the aim to demonstrate the ability of fractal dimension to discriminate between healthy and pathological texture.

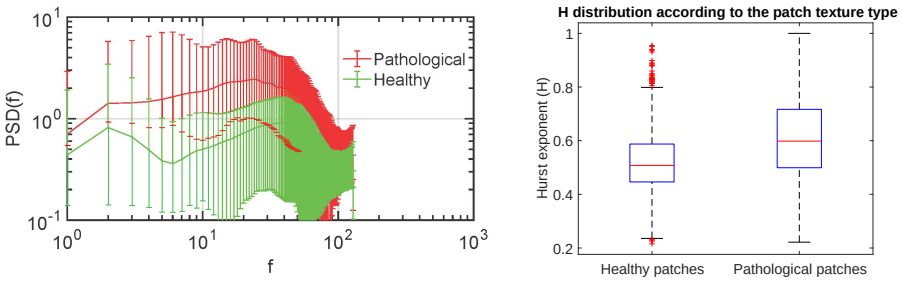

(a) (b)

Figure 7: (a) Average PSD comparison between the two populations, pathological (in red) and healthy (in green) and (b) Hurst exponents ± SD estimated using GSE for the healthy and pathological groups.

To avoid biased results produced by training and testing sets selection, in this work we use an external k-fold cross-validation procedure. For each database under study, the whole dataset composed by N images is divided into k partitions. Then patches extracted from the images belonging to $k-1$ partitions are used for training a classifier as described in Section 2.4.3, and the patches extracted from the remaining partition of images are used for testing. The procedure is carried out k times, leaving out a different partition in each repetition.

The optimal patch size (N_w) and the overlap (Δx,Δy) used to extract the local features were obtained through an internal $v-fold$ cross-validation process with $v = 8$ folds. Note that this technique is applied to the "patch" instances extracted from the fundus images. From this process, a patch size $N_w = 64$ pix. and an overlap (Δx,Δy) $= 32$ pix. were obtained as optimal parameters for the local analysis in the exudate detection task. Regarding to the classification stage, a Radial Basis Function (RBF) kernel was used. RBF kernel is characterised by two parameters (C, γ). The parameter C trades off miss-classification of training examples against simplicity of the decision surface, while the parameter γ defines how far the influence of a single training example reaches. Internal $v-fold$ cross-validation was used in the experiments in order to "grid search" the optimal parameters. Several pairs of (C, γ) values were tried and the one with the highest cross-validation accuracy was selected for each k partition [31].

In addition, the problem of unbalanced data is solved using the Bagging technique with $M = 7$ classifiers. It is important to note that in the test stage, each SVM classifier predicts one label for each patch and the final decision is obtained using a voting algorithm. The individual decision of each classifier is pondered by the probability assigned in the classification. The final assignment of the class is made according to the sum of all weighted decisions. If this sum is greater than 0.5, the patch is classified as pathological texture, while if the sum is less than 0.5 the tissue is classified as healthy. The whole classification strategy is summarized in Figure 8.

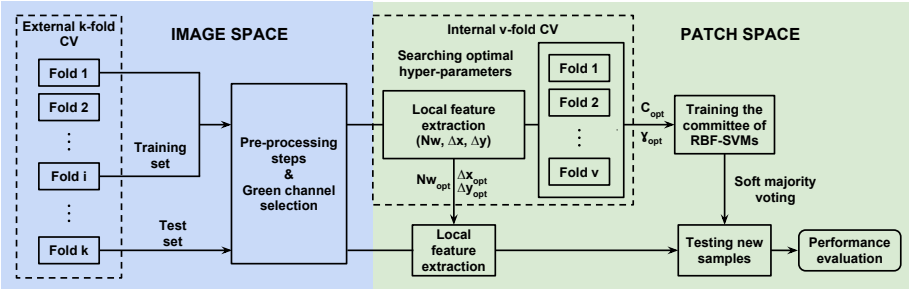

Figure 8: Overview of the classification strategy.

Table 2 shows the evaluation of the classification performance for the two public databases detailed in Section 2.1. The classification of the retina background patches extracted from the 14 images that compose the test set are evaluated by using six metrics. Accuracy (ACC) measures the fraction of correct predictions by the total number of cases. Sensitivity (SENS) and specificity (SPEC) measure the proportion of positive and negative cases which are correctly identified as such, respectively. The positive and negative predictive values (PPV and NPV respectively) measure the proportion of positive (negative) cases classified correctly according to the gold standard and the total number of positive (negative) predictions determined by the classification system. Finally, the area under the ROC curve (AUC) relates the hit rate to the false alarm rate and it is an extended way to measure the predictive modelling accuracy [35]. This measure allows to establish fair comparisons where there is a strong

imbalance between classes [36].

Database	ACC	SENS	SPEC	PPV	NPV	AUC
E-OPHTHA_EX	0.6980	0.6149	0.7488	0.2981	0.9213	0.7168
DIARETDB1	0.8361	0.6047	0.8657	0.3448	0.9459	0.8176

Table 2: Results of the classification patch process using the fractal descriptor.

As we can observe, fractal dimension presents a promising ability to describe patches with lesions allowing the discrimination from the healthy texture. It is important to note that using only two features (the Hurst exponent in two directions), the classifier is able to correctly classify 69.8% of all the instances extracted from the test images of the E-OPHTHA_EX database and 83.61% of all the patches extracted from the test images of the DIARETDB1 database. From the SPEC and NPV measures of Table 2 it is possible to determine the great capacity of fractal analysis for modelling the healthy tissue. Regarding to the sensitivity and positive predicted values, results suggest the difficulty of discriminating a large test set using two features. With the objective of improving this aspect, texture information is incorporated to the feature vector combining the Hurst parameters with another descriptor.

Figure 9 shows the visual representation of the exudate detection in one representative image of each database. In this figure, red squares indicate the true positives, green squares the false positives and the blue squares reveal the false negative detections.

3.3. Fractal dimension combined with Local binary patterns

As we demonstrated above, fractal analysis is able to describe pathological retinal tissues with around 70% and 83% of success in each database under evaluation. However, the SVM classifiers involved in the bagging process are using only two features, the Hurst exponent or fractal dimension in $L = 2$ directions, to perform the discrimination. In order to improve the accuracy of the bright lesion detection, the fractal descriptor is combined with Local Binary

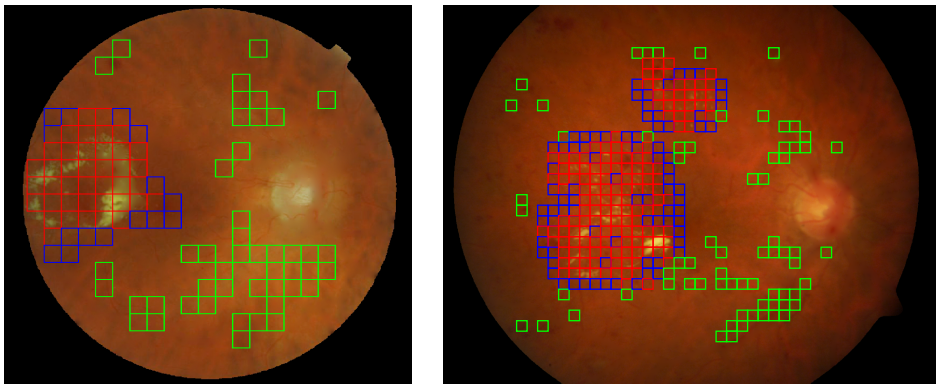

(a) (b)

Figure 9: Automatic exudate detection in two retinal images using the fractal dimension as unique feature. (a) Representative image (DS000U30.jpg) from the E-OPHTHA_EX database and (b) representative image (image014.png) from DIARETDB1 database. Red squares indicate the true positives, green squares the false positives and the blue squares reveal the false negative detections.

Patterns (LBP). LBP is a powerful grey-scale texture operator used in many computer vision applications. This descriptor establishes a label for each pixel taking into account its neighbourhood which is defined by a radius R and number of points P. Many variants of LBP exist in the literature but the rotation-invariant uniform LBP presented in [37] is used in this work. Using this LBP variant, ten different texture labels could be generated depending on the binary string computed in the comparison between a pixel and its neighbourhood. When LBP is used for texture description it is common to include a contrast measure by defining the Rotational Invariant Local Variance [37]. As a novelty in the retina texture description stage, in this work LBP (rotation-invariant uniform variant) and VAR are combined following the process proposed by Guo et al. [38] resulting the LBP variance (LBPV). Both descriptors (LBP and VAR) are computed for the whole image and the normalized histogram of the LBPV is extracted from each patch.

LBPV is computed in a circular neighbourhood of radius $R = 1$ by defining $P = 8$ neighbours. A discrete histogram composed by ten labels or patterns

describes each patch extracted from the images. A new model taking only into account this texture information is trained. Table 3 reports the classification performance obtained for the two databases under study.

Database	ACC	SENS	SPEC	PPV	NPV	AUC
E-OPHTHA_EX	0.7212	0.7947	0.6121	0.4178	0.8603	0.7393
DIARETDB1	0.8229	0.8366	0.7990	0.4212	0.8987	0.8125

Table 3: Classification patch performance using as feature vector the ten patterns of the LBPV histogram.

As can be observed in the previous table, the LBPV descriptor presents a good performance in exudate detection. Using the ten features provided by the LBPV histogram, 72.12% and 82.29% of classification accuracy is achieved for each database. Paying attention to the sensitivity and PPV values, the texture information is able to reduce the number of false positives at expense of a drastic reduction of the true negatives detections. Analysing the results showed in Tables 2 and 3, in particular SENS, SPEC, PPV and NPV measures, it is possible to extract a complementary behaviour between the roughness and texture descriptors. In spite of this complementary behaviour, a similar overall performance in the classification is glimpsed attending to the ACC and AUC measures. This fact is exploited in a second test, in which the ten features obtained from the LBPV histogram computation are combined with the fractal dimension computed in two directions (0 and 90 degrees) composing a feature vector that combines texture and roughness information. The same test as we presented in the previous section is performed achieving the results showed in Table 4.

The fact of feeding the classifier with a combination of texture and contrast information (LBPV) and roughness information (FD) provides a powerful system to discriminate between healthy and pathological retinal tissue. A promising trade-off between sensitivity-specificity and PPV-NPV (Table 4) propitiates higher values of AUC. Based on [39], AUC values greater than 0.85 invites to

Database	ACC	SENS	SPEC	PPV	NPV	AUC
E-OPHTHA_EX	0.8477	0.7478	0.8705	0.4061	0.9528	0.8686
DIARETDB1	0.8987	0.8083	0.9023	0.4175	0.9656	0.8812

Table 4: Classification patch performance using as feature vector the fractal dimension combined with the LBPV histogram.

consider the proposed methodology as a "good diagnostic test" for the hard exudate detection. The robustness of the proposed system against the variability introduced by the use of different image databases is another relevant aspect to emphasize.

The new feature vector provides an accurate bright lesion detection in fundus images. Now, only particular patches composed by less of five percent of pixels with lesion are not identified as pathological tissue. Figure 10 shows the automatic identification of exudates in the same images that in the previous section allowing to observe the improvement by visual inspection.

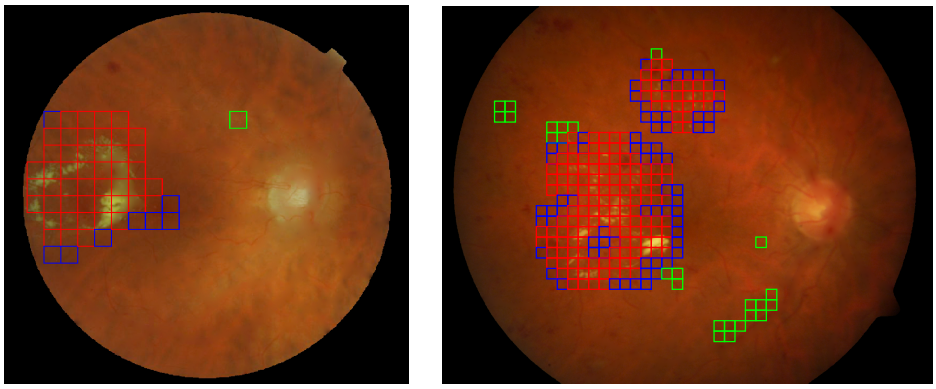

(a) (b)

Figure 10: Automatic lesion detection in two retinal images using the LBPV histogram and the fractal dimension as feature vector. (a) Representative image (DS000U30.jpg) from the E-OPHTHA_EX database and (b) representative image (image014.png) from DIARETDB1 database.

Thanks to DIARETDB1 public database, the proposed method for exudate detection can be compared with some state-of-the-art works, in which, the de-

tection/segmentation of these lesions is performed by using classical techniques such as filtering and mathematical morphology. Table 5 summarizes the exudate detection results achieved by the proposed method and by other works of the literature.

Methods	Sensitivity	Specificity	PPV
Sopharak et al.[40]	0.4348	**0.9931**	0.2548
Walter et al.[1]	0.6600	0.9864	0.1945
Welfer et al.[2]	0.7048	0.9884	0.2132
M.Ghafourian et al.[3]	0.7828	-	-
Proposed method	**0.8083**	0.9023	**0.4175**

Table 5: Comparison of exudate detection methods for the 47 retinal images with exudates of DIARETDB1 database.

The proposed method presents the best trade-off between sensitivity-specificity improving the representative methods involved in the comparison. In Sopharak et al.[40] and Walter et al. [1], poor sensitivity values are achieved. This fact is quite relevant taking into account that this parameter is directly related with the quality of predicting positive instances. Sensitivity value is the unique measure provided by [3] about the performance of its method. Taking into account only one parameter is not possible to establish the goodness of that method. The algorithm introduced by [2] provides interesting results. However, analysing together the three parameters of Table 5 it is possible to observe that our method outperforms the Welfers' one. It is important to note that if AUC parameter would have been included in the works involved in the comparison a more exhaustive comparison would have enabled.

4. Conclusions

In this work, fractional Brownian motion model was used in order to describe grayscale retinal images allowing the estimation of the fractal dimension. With the aim of reliably applying fractal analysis in fundus images, a prepro-

cessing stage combining resizing, inpainting and colour-normalization methods was essential due to the high image variability in the databases. After that, different test were carried out using the E-OPHTHA and DIARETDB1 public databases. The local estimation of the Hurst exponent by linear regression made possible to discriminate between healthy and pathological retinal tissue in a statistical highly significant way ($p<0.001$). This fact led the authors to develop an automatic system able to detect the bright lesions using as feature the fractal dimension and a committee of SVM classifiers. The obtained results glimpsed the need of creating a more robust feature vector able to avoid the possibility of underfitting. The normalized LBPV histograms were extracted from the image patches and new experiments using this descriptor showed a complementary behaviour with respect to the fractal dimension. This fact propitiated a last experiment, in which, the SVM models were recalculated using as feature vector a combination of roughness information, provided by the fractal analysis, and texture information, extracted by the LBPV histograms. This novel approach reached an accurate bright lesion detection. In particular, 85% and 90% of accuracy was achieved in E-OPHTHA_EX and DIARETDB1 respectively. In addition, the proposed system was able to outperform the most representative state-of-the-art methods in exudate detection showing the best trade-off between sensitivity-specificity.

In future research, piecewise fractional Brownian motion model will be explored. In this model, the PSD of the graylevel increments is supposed multifractal, in other words, the spectrum can be divided in fragments and several Hurst parameters will be extracted by linear regressions. Each patch will be represented by a fractal signature. Moreover, the authors would like to explore Minkowski functionals and Minkowski tensors [41] with the aim of extracting new fractal features from fundus images [42]. In addition, fractal analysis will be used to detect red dark lesions as microaneurysms and haemorrhages. This fact would allow to automatically discriminate between two of the most frequent causes of blindness or vision impairment in the world: diabetic retinopathy and age-related macular degeneration.

Acknowledgements

This paper was supported by the the European Union's Horizon 2020 research and innovation programme under the Project GALAHAD [H2020-ICT-2016-2017, 732613]. In addition, this work was partially funded by the Ministerio de Economía y Competitividad of Spain, Project SICAP [DPI2016-77869-C2-1-R]. The work of Adrián Colomer has been supported by the Spanish Government under a FPI Grant [BES-2014-067889]. We gratefully acknowledge the support of NVIDIA Corporation with the donation of the Titan Xp GPU used for this research.

References

[1] T. Walter, J.-C. Klein, P. Massin, A. Erginay, A contribution of image processing to the diagnosis of diabetic retinopathy - detection of exudates in color fundus images of the human retina., IEEE Trans. Med. Imaging 21 (10) (2002) 1236–1243.

[2] D. Welfer, J. Scharcanski, D. R. Marinho, A coarse-to-fine strategy for automatically detecting exudates in color eye fundus images., Computerized Medical Imaging and Graphics 34 (3) (2010) 228–235.

[3] M. Ghafourian, H. Pourreza, Localization of hard exudates in retinal fundus image by mathematical morphology operations, in: 2nd International eConference on Computer and Knowledge Engineering., 2012, pp. 185–189.

[4] K. Harrar, L. Hamami, E. Lespessailles, R. Jennane, Piecewise whittle estimator for trabecular bone radiograph characterization, Biomedical Signal Processing and Control 8 (6) (2013) 657–666.

[5] W. Deering, B. J. West, Fractal physiology, IEEE Engineering in Medicine and Biology Magazine 11 (2) (1992) 40–46.

[6] R. Jennane, W. J. Ohley, S. Majumdar, G. Lemineur, Fractal analysis of bone x-ray tomographic microscopy projections, IEEE Trans. Med. Imaging 20 (5) (2001) 443–449.

[7] G. Landini, Fractals in microscopy, Journal of Microscopy 241 (1) (2011) 1–8.

[8] G. Dougherty, G. M. Henebry, Fractal signature and lacunarity in the measurement of the texture of trabecular bone in clinical ct images., Medical Engineering and Physics 23 (6) (2001) 369–380.

[9] M. Phothisonothai, M. Nakagawa, Eeg signal classification method based on fractal features and neural network, in: 2008 30th Annual International Conference of the IEEE Engineering in Medicine and Biology Society, 2008, pp. 3880–3883.

[10] O. M. Bruno, R. de Oliveira Plotze, M. Falvo, M. de Castro, Fractal dimension applied to plant identification, Inf. Sci. 178 (12) (2008) 2722–2733.

[11] S. Mudigonda, F. Oloumi, K. M. Katta, R. M. Rangayyan, Fractal analysis of neovascularization due to diabetic retinopathy in retinal fundus images, in: E-Health and Bioengineering Conference (EHB), 2015, 2015, pp. 1–4.

[12] T. J. MacGillivray, N. Patton, F. N. Doubal, C. Graham, J. M. Wardlaw, Fractal analysis of the retinal vascular network in fundus images, in: 2007 29th Annual International Conference of the IEEE Engineering in Medicine and Biology Society, 2007, pp. 6455–6458.

[13] M. Z. C. Azemin, D. K. Kumar, T. Y. Wong, R. Kawasaki, P. Mitchell, J. J. Wang, Robust methodology for fractal analysis of the retinal vasculature, IEEE Transactions on Medical Imaging 30 (2) (2011) 243–250.

[14] E. Decencière, G. Cazuguel, X. Zhang, G. Thibault, et al., TeleOphta: Machine learning and image processing methods for teleophthalmology, IRBM 34 (2) (2013) 196–203.

[15] T. Kauppi, V. Kalesnykiene, J. K. Kamarainen, L. L. I. Sorri, A. Raninen, R. Voutilainen, et al., Diaretdb1 diabetic retinopathy database and evaluation protocol, in: Proc. Medical Image Understanding and Analysis, 2007.

[16] B. Mandelbrot, How long is the coast of britain? statistical self-similarity and fractional dimension, Science 156 (3775) (1967) 636–638.

[17] B. B. Mandelbrot, J. W. Van Ness, Fractional brownian motions, fractional noises and applications, SIAM Review 10 (4) (1968) 422–437.

[18] H. E. Hurst, R. P. Black, Y. M. Simaika, Long-term storage : an experimental study / by H.E. Hurst, R.P. Black, Y.M. Simaika, Constable London, 1965.

[19] R. Lopes, N. Betrouni, Fractal and multifractal analysis: A review, Medical Image Analysis 13 (4) (2009) 634 – 649.

[20] I. S. Reed, P. C. Lee, T. K. Truong, Spectral representation of fractional brownian motion in n dimensions and its properties, IEEE Transactions on Information Theory 41 (5) (1995) 1439–1451.

[21] R. J. Barton, H. V. Poor, Signal detection in fractional gaussian noise, IEEE Transactions on Information Theory 34 (5) (1988) 943–959.

[22] A. Eke, P. Herman, L. Kocsis, L. R. Kozak, Fractal characterization of complexity in temporal physiological signals, Physiological Measurement 23 (1) (2002) R1.

[23] P. Flandrin, Wavelet analysis and synthesis of fractional brownian motion, IEEE Transactions on Information Theory 38 (2) (1992) 910–917.

[24] A. Colomer, V. Naranjo, J. Angulo, Colour normalization of fundus images based on geometric transformations applied to their chromatic histogram, in: IEEE International Conference on Image Processing, 2017, article in Press.

[25] S. Morales, V. Naranjo, J. Angulo, J. J. Fuertes, M. Alcañiz, Segmentation and analysis of retinal vascular tree from fundus images processing., in: BIOSIGNALS, SciTePress, 2012, pp. 321–324.

[26] J. D'Errico, Inpainting nans, `http://www.mathworks.com/matlabcentral/fileexchange/4551-inpaint-nans`. Last accessed on 12th January 2016 (2004).

[27] X. Zhang, G. Thibault, E. Decencire, B. Marcotegui, et al., Exudate detection in color retinal images for mass screening of diabetic retinopathy, Medical Image Analysis 18 (7) (2014) 1026–1043.

[28] M. Abràmoff, J. Folk, D. Han, et al., Automated analysis of retinal images for detection of referable diabetic retinopathy, JAMA Ophthalmology 131 (3) (2013) 351–357.

[29] S. Morales, V. Naranjo, J. Angulo, M. Alcaniz, Automatic detection of optic disc based on pca and mathematical morphology, Medical Imaging, IEEE Transactions on 32 (4) (2013) 786–796.

[30] B. Pesquet-Popescu, J. Lévy Véhel, Stochastic Fractal Models for Image Processing, IEEE Signal Procesing Magazine 19 (5) (2002) 48–62.

[31] C. Chang, C. Lin, Libsvm: A library for support vector machines, ACM Trans. Intell. Syst. Technol. 2 (3) (2011) 27:1–27:27.

[32] L. Breiman, Bagging predictors, Machine Learning 24 (2) (1996) 123–140.

[33] F. Yepes, F. Pedregosa, B. Thirion, Y. Wang, N. Lepore, Automatic pathology classification using a single feature machine learning - support vector machines, in: SPIE Medical Imaging 2014, Vol. 9035, San Diego, United States, 2014, p. 24.

[34] R. Mankiewicz, The Story of Mathematics, Cassell, 2000.

[35] J. Huang, C. X. Ling, Using auc and accuracy in evaluating learning algorithms, IEEE Transactions on Knowledge and Data Engineering 17 (3) (2005) 299–310.

[36] R. C. Prati, G. E. A. P. A. Batista, M. C. Monard, A survey on graphical methods for classification predictive performance evaluation, IEEE Transactions on Knowledge and Data Engineering 23 (11) (2011) 1601–1618.

[37] T. Ojala, M. Pietikainen, T. Maenpaa, Multiresolution gray-scale and rotation invariant texture classification with local binary patterns, IEEE Transactions on Pattern Analysis and Machine Intelligence 24 (7) (2002) 971–987.

[38] Z. Guo, L. Zhang, D. Zhang, Rotation invariant texture classification using {LBP} variance (lbpv) with global matching, Pattern Recognition 43 (3) (2010) 706 – 719.

[39] J. A. Swets, Measuring the accuracy of diagnostic systems, Science 240 (4857) (1988) 1285–1293.

[40] A. Sopharak, B. Uyyanonvara, S. Barman, T. H. Williamson, Automatic detection of diabetic retinopathy exudates from non-dilated retinal images using mathematical morphology methods, Computerized Medical Imaging and Graphics 32 (8) (2008) 720 – 727.

[41] Gring, D., Klatt, M. A., Stegmann, C., Mecke, K., Morphometric analysis in gamma-ray astronomy using minkowski functionals - source detection via structure quantification, A&A 555 (2013) A38.

[42] E. Spodarev, P. Straka, S. Winter, Estimation of fractal dimension and fractal curvatures from digital images, Chaos, Solitons & Fractals 75 (2015) 134 – 152.